ASTROBIOLOGY
Volume 2, Number 3, 2002

Application of Hyperspectral Infrared Analysis of Hydrothermal Alteration on Earth and Mars

MATILDA THOMAS* and MALCOLM R. WALTER

ABSTRACT

An integrated analysis of both airborne and field short-wave infrared hyperspectral measurements was used in conjunction with conventional field mapping techniques to map hydrothermal alteration in the central portion of the Mount Painter Inlier in the Flinders Ranges, South Australia. The airborne hyperspectral data show the spatial distribution of spectrally distinct minerals occurring as primary minerals and as weathering and alteration products. Field spectral measurements, taken with a portable infrared mineral analyzer spectrometer and supported by thin-section analyses, were used to verify the mineral maps and enhance the level of information obtainable from the airborne data. Hydrothermal alteration zones were identified and mapped separately from the background weathering signals. A main zone of alteration, coinciding with the Paralana Fault zone, was recognized, and found to contain kaolinite, muscovite, biotite, and K-feldspar. A small spectral variation associated with a ring-like feature around Mount Painter was tentatively determined to be halloysite and interpreted to represent a separate hydrothermal fluid and fluid source, and probably a separate system. The older parts of the alteration system are tentatively dated as Permo-Carboniferous. The remote sensing of alteration at Mount Painter confirms that hyperspectral imaging techniques can produce accurate mineralogical maps with significant details that can be used to identify and map hydrothermal activity. Application of hyperspectral surveys such as that conducted at Mount Painter would be likely to provide similar detail about putative hydrothermal deposits on Mars. Key Words: Hyperspectral infrared analysis—Hydrothermal deposits—Mineralogical mapping—Mount Painter, Australia. Astrobiology 2, 335–351.

INTRODUCTION

ANCIENT HYDROTHERMAL ENVIRONMENTS are prime targets in the search for earliest life on Earth and former life on Mars (e.g., Bock and Goode, 1996). Hyperspectral infrared analysis techniques provide a useful tool in the exploration and mapping of such environments on both planets. Mount Painter in the northern Flinders Ranges of South Australia is one of the largest known terrestrial hydrothermal systems and thus provides a suitable environment in which to explore the application of these techniques. We used a dataset from an airborne hyperspectral short-wave infrared (SWIR) spectrometer to make a mineral map of the Mount Painter Palaeozoic hydrothermal system and then ground-truthed the map using a hand-held spectrometer. We pos-

Australian Centre for Astrobiology, Department of Earth and Planetary Sciences, Macquarie University, North Ryde, New South Wales, Australia.
*Present address: Geoscience Australia, Canberra, Australian Capital Territory, Australia.

tulate that a similar exploration strategy would be highly effective on Mars, in that case using satellite and robotic rover-mounted instruments.

Spectroscopy is the measurement and analysis of portions of the electromagnetic spectrum to identify spectrally distinct and physically significant features of a material (Fig. 1). Spectral data are measured using spectral sensors, which record radiation (usually solar) reflected from the surface of materials. Because many materials absorb radiation at specific wavelengths, it is possible to identify them by characteristic absorption features, which appear as troughs in a spectral curve (Kruse, 1994).

Wavelength ranges most suitable for the discrimination of geological materials include the visible and near-infrared (VNIR), SWIR, and the mid- or thermal infrared (TIR) (Fig. 2). Spectral variation is the result of different compositions, the degree of ordering, mixtures, and the grain size of different rocks and minerals (Table 1) (Huntington, 1996). Owing to their multiple valence states, transition elements, such as Fe, Cu, Ni, Cr, Co, Mn, V, Ti, and Sc, display the most prominent spectral features in the VNIR wavelength range (Kruse, 1994).

The SWIR wavelength region between 2,000 and 2,500 nm is particularly suitable for mineral mapping. The 2,000–2,400 nm wavelength region can show many absorption features characteristic of certain hydroxyl- and carbonate-bearing minerals and mineral groups that are characteristic of hydrothermal alteration. These mineral groups may include pyrophyllite, kaolinite, dickite, micas, chlorites, smectite clays, alunite, jarosite, calcite, dolomite, and ankerite (Linton, 1998).

Using spectroscopy, and in particular hyperspectral imaging technology, it is possible to make accurate maps of surface mineralogy including boundaries, relative abundances, and mineral assemblages. Hyperspectral mapping techniques can identify individual species of iron and clay minerals, which can provide detailed information about hydrothermal mineralization and alteration zones (Huntington, 1996). Hyperspectral remote sensing has a distinct advantage over other remote sensing methods due to its abil-

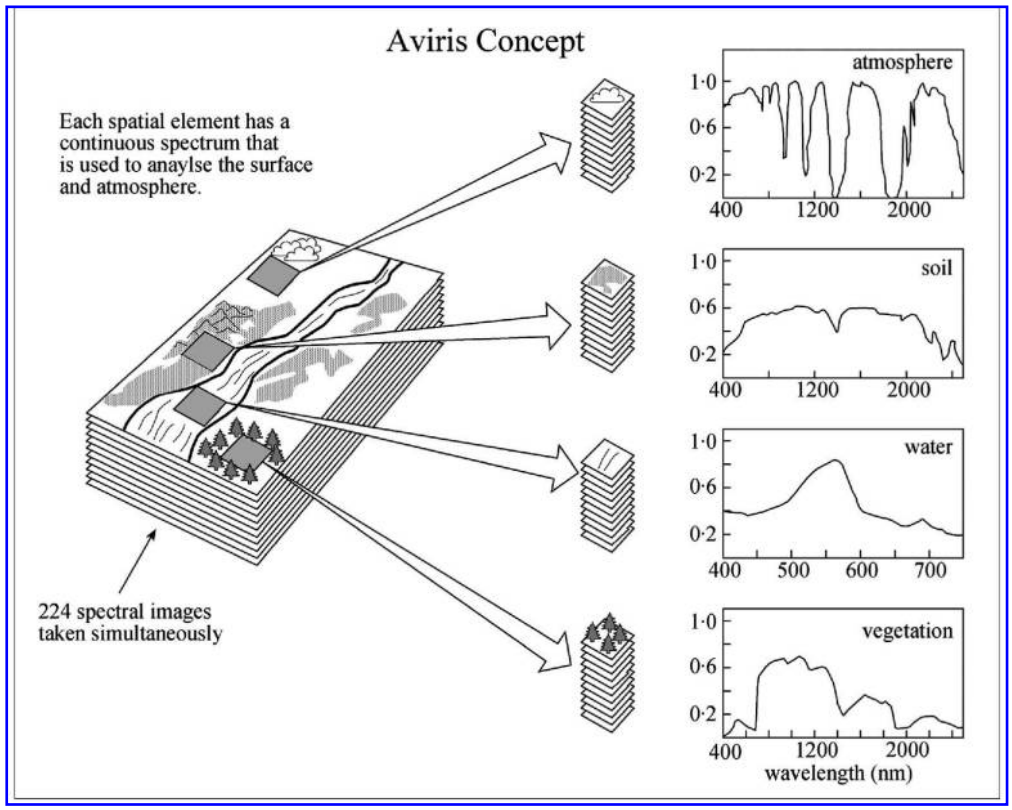

FIG. 1. Schematic diagram of the imaging spectrometry concept. Images are acquired simultaneously of up to several hundred narrow spectral bands, providing a complete reflectance spectrum for every pixel in the imaging spectrometer scene (Courtesy NASA).

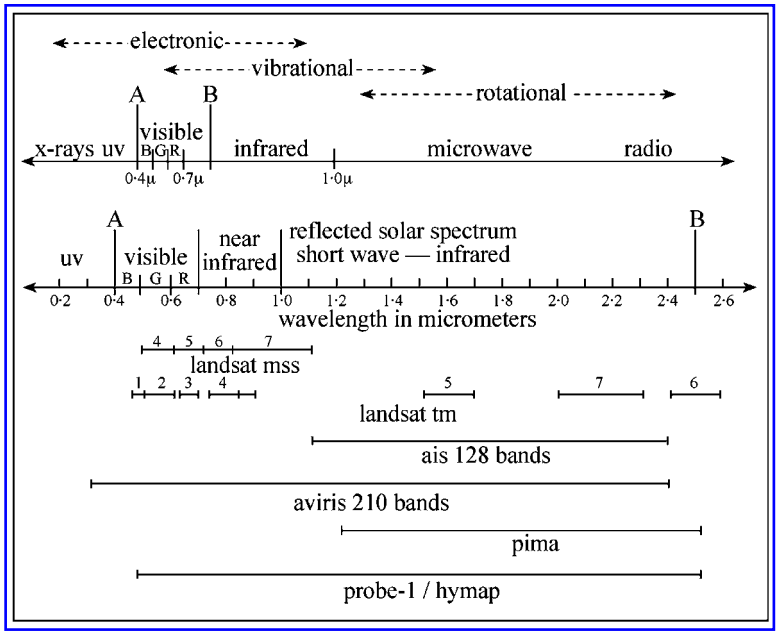

FIG. 2. Electromagnetic spectrum. The top diagram locates various bands in a relative sense, the next line is an expansion of the AB portion. The bottom line shows approximate band locations for some of the operational multispectral and hyperspectral systems (modified from Rinker, 1994).

ity to differentiate fine spectral variations between different types of rock, making it suited to mapping surface lithology (Wang *et al*., 1998). Hyperspectral imaging spectrometers measure and record light reflected from the surface in numerous contiguous channels and using narrow bandwidths (see Fig. 1; Kokaly *et al*., 1998).

Wang *et al*. (1998) showed that using hyperspectral remote sensing techniques, types of minerals and altered minerals that are closely related to the mineralizing process can be determined. Wang *et al*. (1998) also noted that the "formation of altered minerals can be analysed, that hydrothermal mineralised altered zones can be delineated, and industrial deposits can be found directly under favourable conditions" (p. 87) and that "hyperspectral remote-sensing is more effective in identifying earth surface lithology than any other remote sensing technique" (p. 93).

Improvements in hyperspectral technologies have not been limited to remote instruments. Advances in technology have also led to the development of highly accurate, high-resolution field spectrometers such as the portable infrared mineral analyzer (PIMA). By ground-truthing air- and space-gathered data with a high-resolution field instrument, such as the PIMA, the spectral resolution and the accuracy of the classification of the remotely sensed data can be determined. Portable infrared spectrometers are particularly suited to mapping hydrothermal alteration zones, which are typically characterized by layer silicates, including clay minerals. Field portable spectroscopy is a viable and economically feasible tool for accurately determining hydrothermal

TABLE 1. GEOLOGICALLY SIGNIFICANT REGIONS OF THE ELECTROMAGNETIC SPECTRUM (FROM KRUSE, 1994)

Wavelength region	*Wavelength (nm) range*	*Mineralogy*	*Associated molecular feature*
VNIR	400–1,100	Fe and Mn oxides, rare earths	Crystal field absorption charge transfer absorption
SWIR	1,100–2,500	Hydroxyls, carbonates, sulfates, micas, amphiboles	$Al(OH)_2$, $Fe(OH)_2$, $Mg(OH)_2$, NH_4, SO_4 absorption, CO_3
TIR	8,000–14,000	Carbonates, silicates	Si-O bond distortion

alteration in both ancient and active environments (Yang *et al.*, 2000).

GEOLOGY OF THE MOUNT PAINTER REGION

The Mount Painter Province is located in the northern Flinders Ranges, South Australia, at the northeastern margin of the Neoproterozoic-Cambrian Adelaide Rift Complex (Fig. 3). At present the ranges comprise an elevated, rugged terrain rising from the plains of Lake Frome in the east, eventually merging into the plains of the Great Artesian Basin to the north.

The Mount Babbage and Mount Painter Inliers, together with the Broken Hill and Olary Domains, make up the Curnamona Province. This region is an extensional, probably back arc, continental margin magmatic area of Paleoproterozoic to Mesoproterozoic age. Neoproterozoic-Cambrian clastic sedimentary and carbonate rocks of the Adelaide Rift Complex unconformably overlie the older succession (Foster *et al.*, 1994). The Mount Painter Inlier comprises crystalline basement rocks, the Mount Painter complex, which includes Palaeo- to

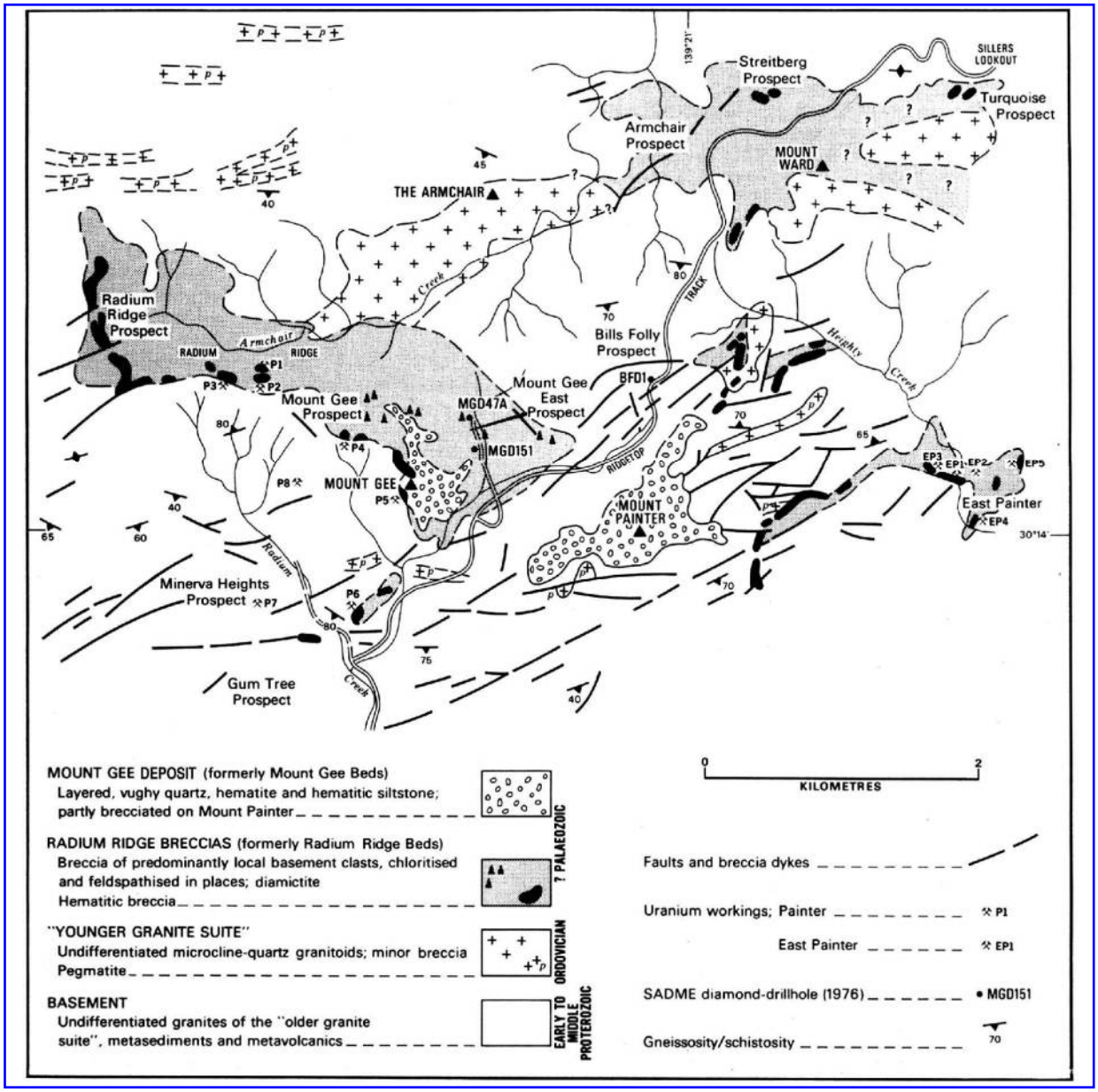

FIG. 3. Geology of the Mount Painter and Mount Babbage Inliers. The various suites are continuous, extending from high to lower metamorphic grade areas, around folds, across major faults and zones of geophysical discontinuity, and through areas that have been subjected to intense retrograde deformation (Drexel and Major, 1990).

Mesoproterozoic metasediments and metavolcanics (the Radium Creek Metamorphics), and Mesoproterozoic granites, pegmatites, and minor amphibolite dykes. Ordovician granites and pegmatites make up a "younger granite suite," which intrudes into the Proterozoic basement. The third component is a convoluted and puzzling collection of breccias, of which a granitic breccia is the most common (Fig. 3). Many of these breccias contain uranium and minor sulfide mineralization and are cemented with hematite. The breccias occur as irregular bodies within the basement complex, adjacent to a zone of extensive faulting, which also contains Ordovician granites and pegmatites (Lambert *et al*., 1982). The breccias have been assigned an age of 280 Ma using palaeomagnetic dating methods (Idnurum and Heinrich, 1993).

A fault system, the Paralana Fault zone, consisting of northeast-trending faults, runs along the eastern margin of the Mount Painter Inlier (Fig. 3). The Paralana Fault zone is generally believed to be the main conduit for hydrothermal fluid dispersal. The fault zone has been intermittently active since the Neoproterozoic formation of the Adelaide Rift Complex; seismic studies suggest the area is still active (Wellman and Greenhalgh, 1988; Foster *et al*., 1994). A modern hot spring (Paralana Hot Springs) is evidence of continuing hydrothermal activity along the Paralana Fault zone. The source of this fluid, and of past hydrothermal fluids, is difficult to ascertain, although it is most likely to be predominantly meteoric in origin (Foster *et al*., 1994).

Apatite fission track analyses (Foster *et al*., 1994) confirm that significant hot spring activity occurred along the Paralana Fault zone during the mid-Tertiary, ending with a stage of uplift during or after the Miocene. Mid-Tertiary hydrothermal activity caused mineralization at depth and redistributed earlier mineralized zones in the Mount Painter Inlier (Foster *et al*., 1994). However, the main time of hydrothermal activity is considered to be Permo-Carboniferous, based on fitting the directions of remanent magnetism in hydrothermal minerals to the apparent polar wander path.

Table 2. Minerals Identified by PIMA II Measurements in the Field Area

Kaolinite	Muscovite
Biotite	Montmorillionite
Phengite	Intermediate chlorite
Phlogopite	Chlorite
Halloysite	Fe chlorite
Calcite	Palygorskite
Epidote	Nontronite
Gypsum	Paragonite
Illite	Jarosite

GROUND OBSERVATIONS

The area of interest for field study extended >100 km^2, and ground observations and sampling, using a PIMA II spectrometer, was conducted over an area of >50 km^2. Some of the minerals identified in the field using the PIMA are listed in Table 2. The PIMA utilizes SWIR, having 601 contiguous spectral bands in the 1,300–2,500 nm wavelength range. The PIMA has a 2-nm sampling interval with ~10 nm resolution; this is high enough to identify subtle absorption features that can impart important information, such as the degree of crystallinity and discrete mineralogical–chemical variations.

Table 3. PIMA II Attributes Versus PROBE-1

PIMA II	*PROBE-1*
• High spectral resolution in the SWIR bands (laboratory-quality spectra)	• Fast and efficient wide area imaging for mineral mapping and environmental monitoring
• Measures 601 contiguous spectral bands from 1,200 to 2,500 nm	• 128 contiguous spectral bands in the 450–2,500 nm range
• Signal-to-noise ratio of 3,500:1	• Signal-to-noise ratio of >500:1
• 1 cm spatial sampling	• 2–10 m spatial resolution
• Built-in wavelength calibration target	• Pre- and/or postflight wavelength and radiometric calibration
• Can run on both Palmtop and Laptop computers	• Operates in any light aircraft equipped with a standard camera port
• Can provide a spectral analysis in the field in 1–3 min	• Can be customized to user requirements

The PIMA data were collected to provide ground-truthing for the airborne data, which were collected using a PROBE-1 instrument. The main differences between the two instruments are listed in Table 3.

PIMA field spectral measurements were made, and hand-samples were collected of rocks that displayed typical mineralogy for each major outcrop area. A total of 78 spectra were obtained from 60 samples. Preliminary processing was carried out in the field using PIMA View software on a Palmtop computer. Background spectra were removed to obtain hull-quotient spectra that could then be used to determine the second-derivative spectra to enhance spectral features and facilitate preliminary identification of minerals (Fig. 4).

Most rocks are made up of mixtures of minerals in varying proportions. Multiple mineralogies may cause overlapping of absorption features, making the spectra difficult to interpret. Second-derivative spectra are crucial in the interpretation of minor and overlapping absorption features, particularly when coupled with a complex background (Yang *et al.*, 2000). The PIMA data were processed using The Spectral Geologist software, which identifies spectra by comparing sampled spectra with extensive spectral libraries.

AIRBORNE OBSERVATIONS

The main aims for processing were to focus on hydrothermal alteration mineral assemblages and to highlight end-member relationships. Mapping alteration minerals and abundances around Mount Painter and Mount Gee was aimed at finding mineralization patterns that could be used to interpret different hydrothermal episodes. Another aim was to try to identify alteration assemblages that could be considered characteristic of a hydrothermal system. The data set, courtesy of Anglo-American Corporation in Johannesburg, was collected by the Australian-designed hyperspectral airborne imaging spectrometer PROBE-1 (also called Hymap). PROBE-1 has 128 channels in the VNIR and SWIR. The PROBE-1 data were collected in 3.2-km-wide swaths of varied lengths (average = 20 km) flown at ~2,200 m (Fig. 5 shows the location of the swaths). Each swath, once corrected and calibrated, has 128 reflectance bands that can then be used for further processing. Corrections, including mean terrain height calibrations, mean aircraft height calibrations, and atmospheric (including water vapor) corrections, were performed using an ATREM-based program called Hycorr developed at CSIRO North Ryde. This preliminary processing reduces the data to the apparent surface reflectance, the most useful for geological mapping purposes.

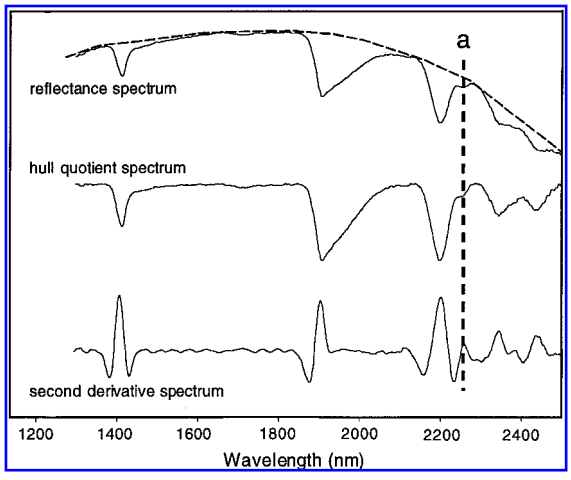

FIG. 4. Examples of reflectance and hull-quotient spectra. A baseline is fitted to the spectral curve (thin dashed line). The spectrum is normalized to this line to remove the effect of a spectral background, producing the hull-quotient spectrum. Note that the minor feature, a, becomes more pronounced on the second derivative spectrum (from Yang *et al.*, 2000).

Processing was performed using ENVI v3.2 software (ENvironment for Visualizing Images), which is specifically designed for image processing of satellite and aircraft remote-sensing hyperspectral data. ENVI is suitable for processing hyperspectral data because of its many unique interactive analysis tools and multiple dynamic overlay capabilities. One particularly useful feature of the ENVI software is that it allows users to make and apply their own customized analysis strategies. Only the SWIR data from 2,000 to 2,500 nm (SWIR2) were used because this range is the most suitable for studying alteration minerals; a SWIR2 subset was used for the following processing method applied separately to each swath:

1. Creation of an albedo mask to eliminate possible complications from nongeological features
2. Normalization of the data to remove per pixel albedo variation
3. Minimum noise fractionation transformation—to de-correlate and order the spectral bands according to a decreasing signal-to-noise ratio (spectral reduction); uses only good pixels to drive statistics; compresses the data

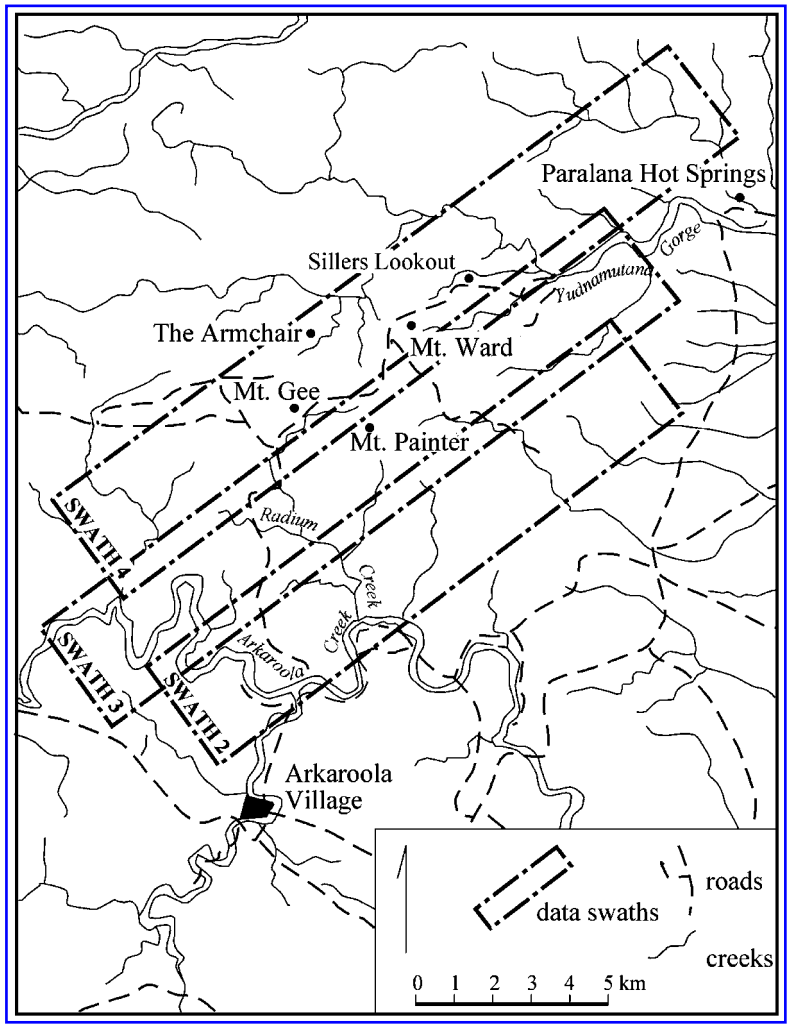

FIG. 5. Location of PROBE-1 data swaths, each 3.2 km wide. The survey was flown in a north–east/south–west direction.

4. Hyper pixel purity index for spatial data reduction—finds spectrally purest pixels in the data by making repeated projections in *n*-dimensional scatter plots onto a lower-dimensional subspace
5. *n*-dimensional visualizer rotates the pixels through *n*-dimensions, producing an animated data cloud by random projections of *n*-dimensional space; end-members found and identified
6. Creation of regions of interest (ROIs)
7. Creation of spectral library of end-members representing the spectrally purest pixels
8. Location of known material in an unknown background—mixture-tuned matched filtering
9. Redefinition of ROIs based on low infeasibility and high matched filtering scores (gives distribution and abundance maps for end-members)
10. Make ROI masks—one for each end-member
11. Vectorization of ROIs using CSIRO's in-house custom mask creation program designed specifically to automate the creation of vectors from ROIs
12. Selection and arrangement of vector layers of end-members to be shown on the final map

The mineral compositional end-member distributions are superimposed onto a base image (a SWIR band) to provide a reference to the ground surface. Like the PIMA, PROBE-1 provides enough resolution to differentiate between types of micas. Comparisons with PIMA data were used to check these minor spectral variations to see if they had geological significance. In Swath

3, a ring-like structure displays a muted spectrum, similar to both kaolinite and halloysite. The identification of halloysite is tentative, but PIMA samples from the same area also identified a halloysite variant that is spectrally different from the other kaolinites in the area. Although the spectra are extremely similar, it is interesting to note that the two variations have distributions that correlate with (1) a possible maar structure centered on Mount Painter with a halloysite variant and (2) a probable later stage of hydrothermal activity associated with the Paralana Fault with the regular kaolinite. Figure 6 shows the different abundances for the two kaolinites (green = possible hallosite variant, yellow = regular kaolinite) identified in Swath 3. Analysis of minimum noise fractionation images revealed a ring-like feature, possibly the physical boundary of a maar structure associated with an extensive first stage of alteration; and a second feature showing a distinctive diagonal linear feature (yellow) that corresponds with the Paralana Fault, interpreted as a second subsequent stage of alteration in the region. More detailed geophysical information is needed to confirm the presence and structure of the proposed maar.

GROUND AND AIRBORNE DATA RESULTS COMPARISON

Correlations between thin-section observations and the PIMA results are generally excellent, with most of the identified PIMA minerals being easily located in thin section, and vice versa. The classification made by The Spectral Geologist software was confirmed by detailed manual inspection of the PIMA spectra. In the case of the many samples containing white micas, the PIMA not only registered a spectrum diagnostic of mica, but was able to make a more detailed classification based on crystallographic structure. The PIMA is able to differentiate between types of micas and between pure muscovites and muscovites with significant amounts of large cation substitution (aluminium replaced by iron or magnesium) in the crystal lattice (K. Yang, personal communication, 2000). In most cases, if a careful choice is made in selecting a representative sample for measurement, the PIMA will provide useful mineralogical data.

While the PIMA produces laboratory-quality spectra, PROBE-1 data do not have the same spectral resolution. PROBE-1 is designed for regional surveys, and PIMA provides ground truth, so greatly enhancing the accuracy of the mineralogical interpretations. The PIMA II field spectrometer confirmed the main mineralogies identified by the airborne survey and provided more detailed mineral information that could be extracted from the PROBE-1 images. The PIMA was also able to confirm the 5-m spatial resolution of PROBE-1 by identifying and mapping a mica-rich rock unit that had been uncovered by the building of a road-cutting. A distinct mica end-member was mapped that correlated with the 5-m-wide road (as seen on aerial images). This section of road was observed in the field to have uncovered a highly micaceous rock that occurred only in this road cutting, and only for the 5-m width of the road.

Two or more minerals can often be inferred from indications in PIMA spectra. The same is true for PROBE-1 data, but separating out individual minerals is even more difficult as several minerals typically occur together in a landscape and can appear as overlapping and "mixed"—this is enhanced by the lower spatial resolution of the airborne dataset. The PIMA II analyses agreed with many of the minerals identified using PROBE-1. The PIMA data also helped support the sometimes difficult unmixing of spectra and mineral identification made with the PROBE-1 data. The advantage of the PROBE-1 data is the facility of detailed regional-scale mapping. Being able to map minor mineralogical variations, such as the mica end-member discovered along the road-cutting, makes this type of airborne survey well suited to mapping surface geology and, in particular, geological features such as alteration zones. The ability to map large areas, particularly in a region with rugged terrain such as the Flinders Ranges, has made possible detailed mineralogical mapping for every 5–10 m^2 of the ground surface. The general agreement between different data types is sufficient to confirm PROBE-1's spatial and spectral resolution and thus the accuracy of the end-member maps.

OTHER ASPECTS OF THE HYDROTHERMAL DEPOSITS

Native sulfur on Mount Painter

An intriguing yellow outcrop was sampled at stop 511.3 (342°150′E 54°800′N) on the northern

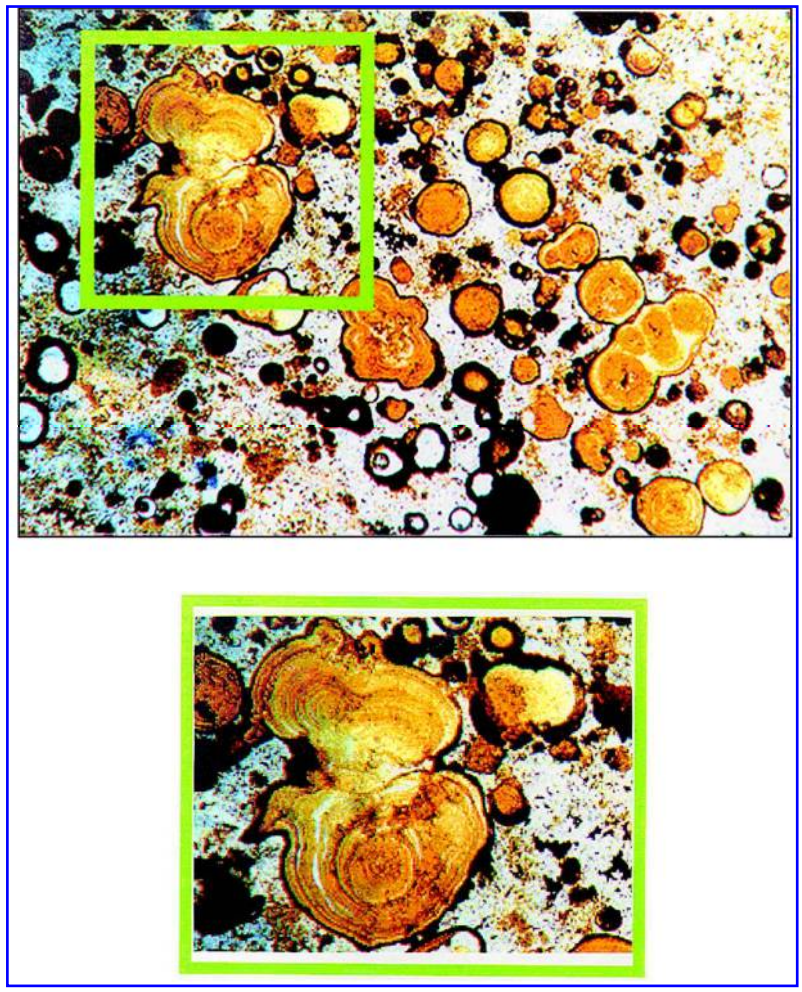

FIG. 6. (**a**) Botryoidal sulfur, alternating bands of silica (clear) and sulphur (yellow). (**b**) Enlargement from photograph above showing banding and botryoidal texture.

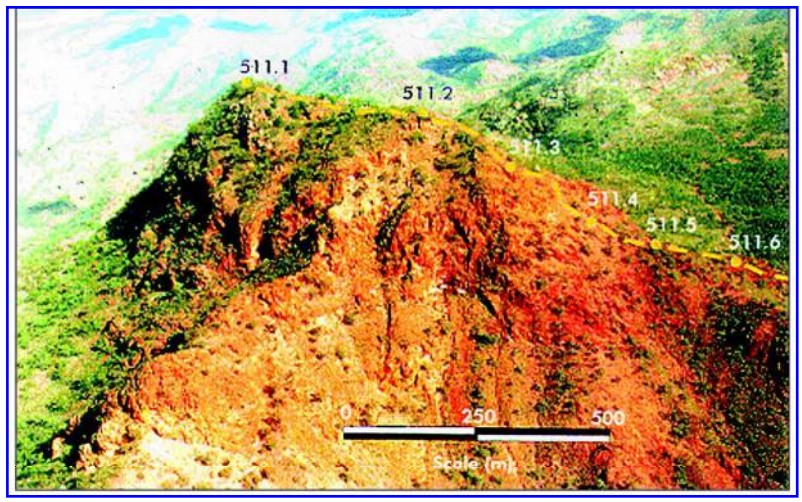

FIG. 7. Looking southwest to Mount Painter showing sample locations. Route starts at southern flank behind and below 5111.1. Scale is approximate only.

side of Mount Painter (see Fig. 7 for location). This outcrop, only some 4–5 m^2, has not previously been reported. Three samples were collected, spectrally analyzed, and thin-sectioned. Analysis of the PIMA data using The Spectral Geologist software registered "null," because the principal rock component is quartz, which has no diagnostic spectral feature at PIMA wavelengths. Petrographic study of two of the samples revealed extensive recrystallization of silica (probably originally chalcedonic), and laminations, vugs, cavity-fill, displacive and pervasive replacement textures in silica, and concentrically banded and botryoidal structures (see Fig. 8). Electron microprobe analysis of the yellow material in the laminations and botryoidal microstructures identified "native" sulfur, with the rest of the scanned image being silica, and minor iron. The electron microprobe results show that the sulfur is not associated with either the iron or the silica. The sulfur occurs in a <2-mm band in sample MU58919. Laminations, some of which are disjointed or broken, appear to have undergone brittle, and possible some minor ductile, deformation.

The presence of native sulfur suggests highly acid oxidizing conditions, typical of the conditions that are found associated with solfataras, steaming grounds, and hot springs.

Origin of sulfur banding

Sulfuric acid can be produced naturally by (a) inorganic and bacterial oxidation of sulfides, (b) disproportionation reaction of sulfur dioxide in magmatic hydrothermal systems, or (c) acidic brines in crater lakes on top of active volcanoes (Kusakabe *et al*., 2000). Mechanism c has been documented in acid sulfate hydrothermal alteration systems but is more typically associated with a crater lake and volcano. The banded sulfur rock samples MU58919 and MU58921 in hand-sample and in thin section show sedimentary characteristics such as graded bedding and soft-sediment deformation structures akin to the banded sulfur rocks described by Kusakabe *et al*. (1986, 2000).

Unbound sulfur is stable under relatively high redox potentials, low temperatures, and high total sulfur concentrations, while hydrogen sulfide is stable only under low redox potentials, high temperatures, and low total sulfur concentrations (Kusakabe *et al*., 2000). High-temperature saline fluids from magma interact with overlying crystalline rocks at different levels and times during the evolution of a system, and can lead to suitable conditions for high sulfidation ore deposits (Kusakabe *et al*., 2000). Strongly acidic fluids produced by SO_2 disproportionation or inorganic oxidation of sulfides produce acid alteration of country rocks. Crater-lake bedded sulfur sediments are the closest match to the bedded and botryoidal sulfur rocks at Mount Painter (Kusakabe *et al*., 1986, 2000), although banded sulfur deposits are common in advanced argillic alteration zones and other hot spring precipitates and surface encrustations. Other comparable materials are the "tiny spheres of sulfur" (Francis *et al*., 1980) and "elemental yellow sulfur coatings" on sand grains from high-temperature hydrothermal vents off the island of Milos, Greece (Dando *et al*., 1998).

Most of the silica was probably deposited in a cryptocrystalline form, or as a gel, as in modern hydrothermal systems (Cady and Farmer, 1996). The jasperoidal unit at Mount Gee could have been deposited as a gel (e.g., Eugster and Jones, 1967), and many textures in the Mount Painter and Mount Gee quartzes are similar to the botryoidal silica surfaces observed at the Sleeper deposit in Nevada (Saunders, 1994), or the recrystallized silica gels from Yellowstone National Park (Fournier *et al*., 1991).

Carbon and oxygen isotope analyses

Results for carbon and oxygen isotope analyses are shown in Fig. 9. The chart includes 23 analyses presented in a paper by Lambert *et al*. (1982) and a sample from Sunshine Pound analyzed for this project. The analyses are from calcite in various hydrothermally altered rock types around the central area of the Mount Painter region. The $\delta^{13}C$ ranges from $-22.3‰$ to $-3.3‰$, and $\delta^{18}O$ from $-4‰$ to $+23.1‰$. There is no apparent systematic change of isotopic composition with location or drill hole depth, and the wide spread of values is probably caused by mixing of two different waters containing CO_2[1] from different sources. The results are consistent with an inverse $\delta^{13}C/\delta^{18}O$ relationship, confirming a mixed origin of the fluids (Lambert *et al*., 1982).

Most calcite samples from the Mount Painter breccias have $\delta^{13}C$ less than $-10‰$, which suggests CO_2 generated from organic carbon (Lambert *et al*., 1982). The higher $\delta^{18}O$ values in the more strongly ^{13}C depleted samples correspond

with values expected for precipitation from fluids derived from argillaceous (carbonaceous) metasediments, as a result of melting or high-grade metamorphic processes. This type of fluid, with $\delta^{18}O$ around +12‰, could produce hydrothermal carbonate with a $\delta^{18}O$ of +23‰ at a temperature of around 170°C (Lambert *et al.*, 1982).

It is likely that the CO_2 was derived by solution of magmatic carbonate minerals and from atmospheric gases in groundwater (Lambert *et al.*, 1982). The sample analyzed in this study, from the Sunshine Pound calcite, has a $\delta^{13}C$ value of −3.3‰ and $\delta^{18}O$ value of −1.3‰. Although the $\delta^{13}C$ value is the highest, the Sunshine Pound values plot well into the category of probable evolution from meteoric waters. Fluctuations in temperature of precipitation of the minor carbonate quantities in the Mount Painter samples can account for the scatter of compositions around the mixing line.

DISCUSSION

The spectral maps of clays, carbonates, and micas reveal information not previously recorded. These maps show alteration zones around Mount Painter and the fault, which can be considered indicative of different mineralization styles and, thus, different fluid chemistries. The abundances of two kaolinite end-members shows that although they overlap, they also occur separately and delineate different features. The features are interpreted as being due to different hydrothermal fluids rather than weathering because they include typical hydrothermal mineral associations. There must also be weathering products present, but more work will be required to differentiate them.

Spectral changes in clay minerals, muscovites, biotites, carbonates, and chlorites were used to map alteration minerals and to identify different mineralogical zones that could relate to different hydrothermal episodes and/or systems.

Mount Painter/Mount Gee can be classified as an epithermal hydrothermal system on the basis of characteristic features: typical epithermal minerals kaolin, pyrophyllite, and zeolites; chalcedonic (although now recrystallized) silica; vuggy silica; and lattice textures produced by silica pseudomorphs of bladed calcite. Vuggy silica, extensive in the Mount Gee hydrothermal quartz unit, can be a good indicator of high-sulfidation deposits (Heald *et al.*, 1987; White and Hedenquist, 1990), but vein and other textural information, combined with the scarcity of sulfides, suggests that the Mount Painter system is a low-sulfidation system (Table 4). Chalcedony indicates local silica saturation and suggests that boiling may have occurred. A temperature of between 190°C and 100°C and a depth of <100 m below the water table is required for its deposition. Chalcedony also indicates, owing to its cryptocrystalline nature, rapid cooling (Clark and Govett, 1990; White and Hedenquist, 1990). The former presence of bladed calcite is consistent with this interpretation.

Changes of mineralization characteristics within the study area are interpreted to be the result of two different hydrothermal fluids from different sources.

Figure 10 shows a conduit structure that permits systems with both separate and shared fluid conduits. It would be expected that any natural fluid conduits would be utilized by both systems. The repeated and overprinted alteration in the area makes it difficult to separate hydrothermal systems or fluid types. However, petrographic differences are enough to assume significantly different fluids and hydrothermal conduit systems.

MARTIAN ANALOGUE

The majority of exploration outside Earth has been, and will at least for the next few decades, continue to be via remote means. Mars is a focus for planetary research, as well as a prime target in the search for extraterrestrial life.

NASA's Thermal Emission Spectrometer instrument that was flown on the Mars Global Surveyor mission detected an extensive deposit of crystalline hematite (α-Fe_2O_3). The deposit covers an area of 350 × 350–750 km, has sharply defined boundaries, and is centered near Sinus Meridiani at 2°S latitude between 0° and 5°W longitude (Cristensen *et al.*, 2000). Positive identification of crystalline hematite requires the presence of fundamental absorption features centered near 300, 450, and >525 cm^{-1} and the absence of silicate fundamentals in the 1,000 cm^{-1} region (Cristensen *et al.*, 2000). A radiative transfer model was used to remove atmospheric interference from CO_2, dust, and water ice. To

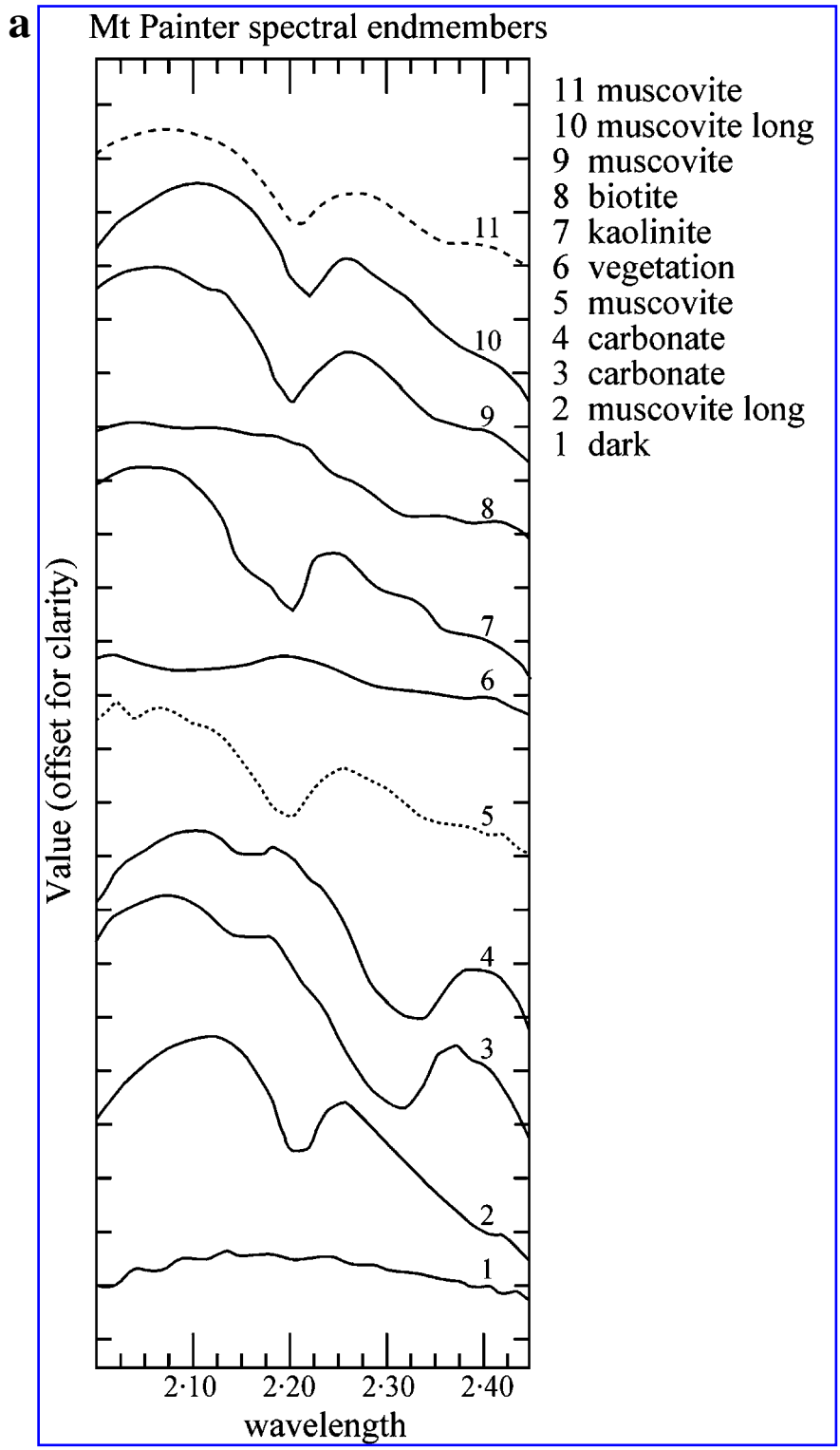

FIG. 8. Mount Painter spectra and endmember maps. (**a**) Identified end-member spectra, including variants of the one mineral. (**b**) Black and white background image is a shortwave infrared band included to provide reference to the ground surface. The endmember maps were created using ENVI 3.2 software.

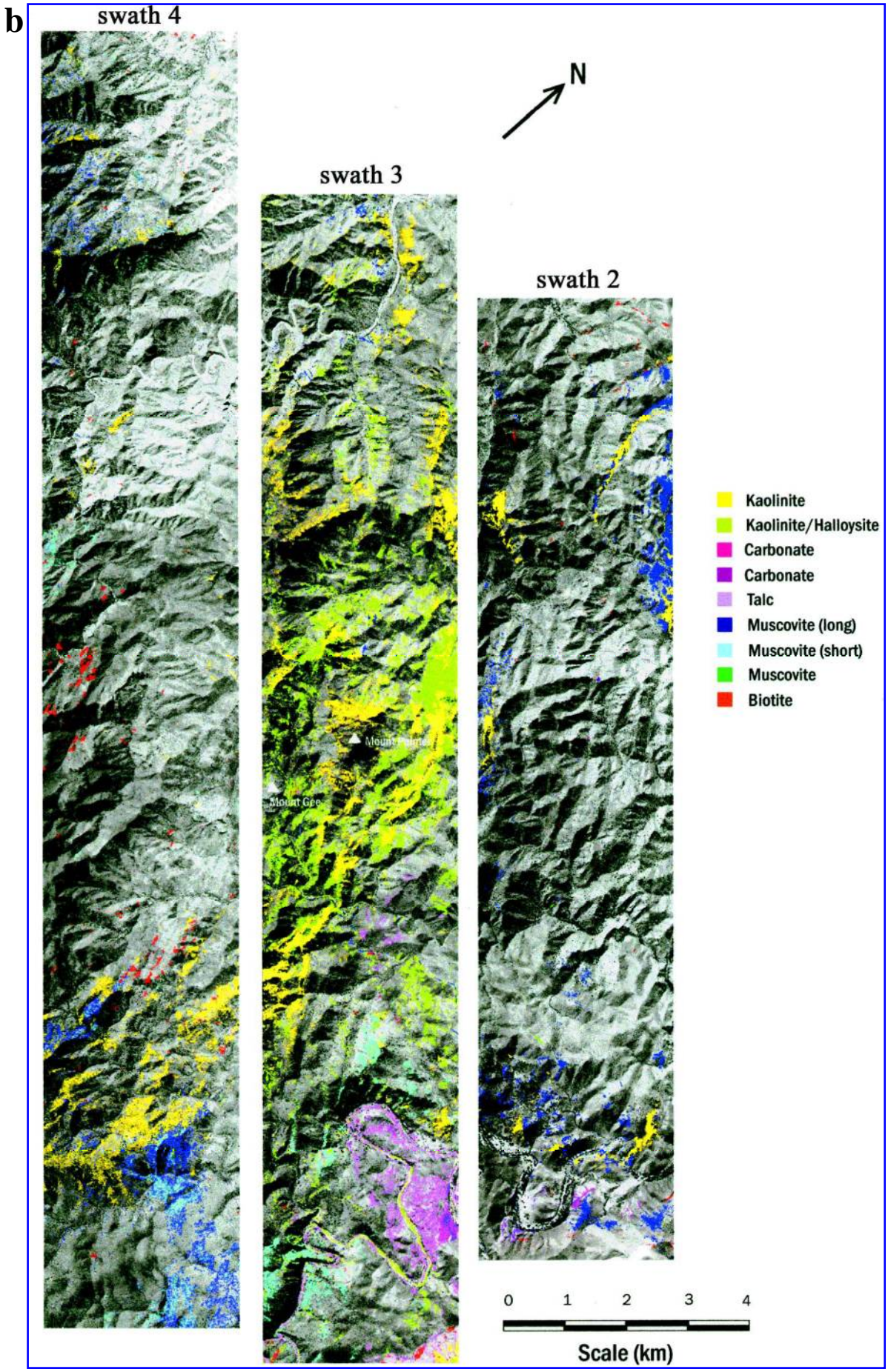
b
swath 4
swath 3
swath 2
N
Kaolinite
Kaolinite/Halloysite
Carbonate
Carbonate
Talc
Muscovite (long)
Muscovite (short)
Muscovite
Biotite
0
1
2
3
4
Scale (km)

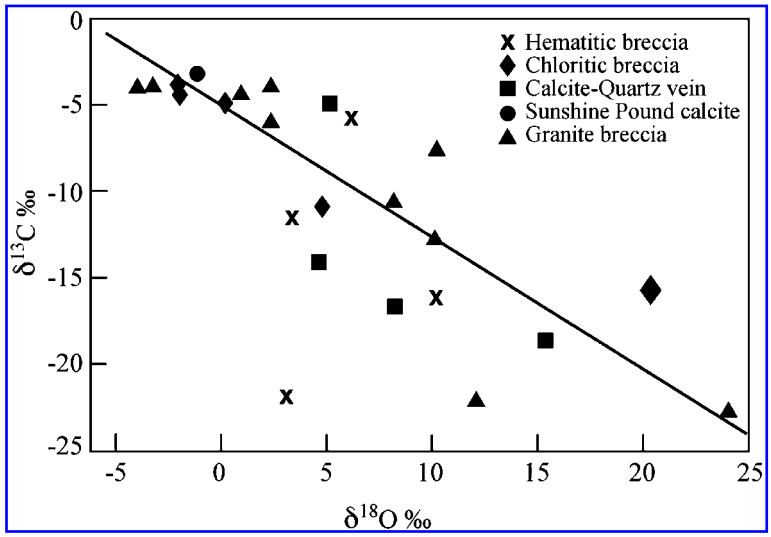

FIG. 9. Carbon and oxygen isotope analyses. Breccia and calcite-quartz vein analyses are from Lambert et al. (1982). Sunshine Pound calcite analyses are from this study.

TABLE 4. DISTINCTION BETWEEN HIGH- AND LOW-SULFIDATION SYSTEMS [MODIFIED FROM WHITE AND HEDENQUIST (1990) AND CORBETT AND LEACH (1994)]

	Low sulfidation	*High sulfidation*
Fluid	Low salinity H_2S-dominant Reduced	Mostly low, some high salinity SO_2-dominant Oxidized
Alteration	Generally neutral alteration adjacent to structures dominated by sericitic/illitic clays ⇨ peripheral propylitic veins dominated by quartz ± carbonate[1] Intensive white mica in regions with high water:rock ratios[1]	Characteristic zoned pervasive acid alteration from: residual (vuggy) quartz ⇨ alunite ⇨ kaolin minerals ⇨ illite minerals ⇨ propylitic[1–4] Deep deposits show intense pyrophilite-white mica alteration Near surface deposits may have pervasive clay alteration[1–3]
Associated minerals	Low % pyrite Galena, sphalerite. chalcopyrite[3]	High % pyrite Engarite–luzonite
Metals: economic accessory	Au ± Ag Pb, Zn, Cu As, Te, Hg, Sb at high levels	Au ± Cu As Te at high levels
Character of mineralization	Veins common with crystalline phases at depth, banded at shallow levels[3]	Hosted in clasts or matrix in competent wall rock alteration[1–4]
Characteristic textures	Crustification,[2,3] banding,[3] colloform banding (S),[2] chalcedony,[2,3] vugs,[2,3] vein breccia,[1,3,4] silica pseudomorphs after bladed calcite[1,3,4]	Vuggy silica (fine-grained quartz)[2,3] Massive silica (fine-grained quartz)[1–4]
Structure	Preexisting fractures at depth subsidiary dilational structures at higher levels Magmatic, diatreme, and eruption breccias[2–4]	Dilational structure and permeable lithological control[3] Diatreme breccias common[3,4]

[1]Present elsewhere in field area.
[2]Present at Mount Painter.
[3]Present at Mount Gee.
[4]Present at Radium Creek.

enhance the unique spectral features at Sinus Meridiani the average neighboring spectrum was removed. The depth and shape of the fundamental bands indicate that the hematite is crystalline and relatively coarse-grained (>5–10 μm) and thus separate from the fine-grained (diameter <5–10 μm), red, crystalline hematite that is considered to be a minor spectral component in Martian bright regions like Olympus-Amazonis (Morris *et al.*, 1997; Cristensen *et al.*, 2000).

The large hematite deposit at Sinus Meridiani could have been deposited from hydrothermal fluids. The deposit may represent a deposit formed by an ancient thermal plume, which periodically welled up at the surface. The phenomenon responsible for the vast size of Martian volcanoes, like Olympus Mons, is the apparent lack of plate tectonics. This same phenomenon could also be used to explain the very large size of the proposed hematite deposit at Sinus Meridiani. Other candidates for hydrothermal deposits have also been recognized (Cady and Farmer, 1996).

CONCLUSIONS

Integrated analysis of both air- and ground-collected SWIR hyperspectral measurements can be applied to interpreting hydrothermal alteration in arid regions of Australia. This study suggests that it would also be possible to apply similar techniques to searching for hydrothermal alteration products on the surface of Mars. Current technology is already at a level where airborne or spaceborne hyperspectral measurements of Mars could be collected and would produce similar levels of detail about surface mineralogy as in this study.

Mapping ancient hydrothermal systems with hyperspectral imaging techniques is effective and can provide detailed information. The ability to map minor spectral features in alteration assemblages can identify structures that would be difficult to locate using other techniques. The hyperspectral maps produced show distinctive areas of mineralization commonly associated with the Paralana Fault zone. The Paralana Fault zone

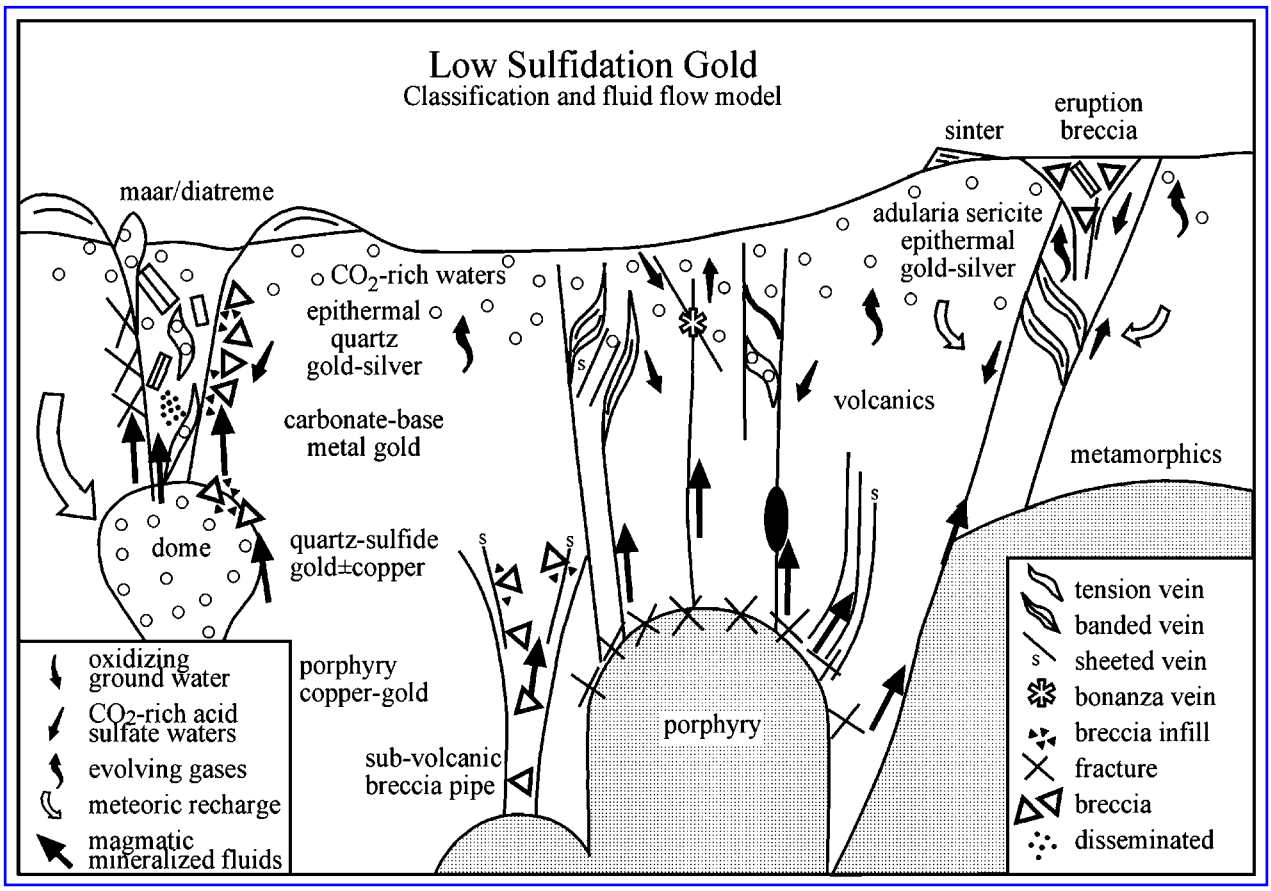

FIG. 10. Low Sulfidation Gold Classification and Fluid Flow Model. From Corbett and Leach (1994).

is still likely to be the most prolific and active hydrothermal fluid conduit, but mineralogical and hyperspectral evidence suggests it is not the only hydrothermal system in the area. The combined PROBE-1 and PIMA II hyperspectral data suggest there is some evidence for two different hydrothermal fluids, responsible for the interpreted mineral variations.

We propose a model with two separate (but adjacent) hydrothermal systems, each with many stages. The first is an extensive adularia-sericite type system that produced hydrothermal fluid alteration mainly along the Paralana Fault zone. It is possible that this system had a fluid of mixed origin as indicated by the C- and O-isotope analyses. The second, a localized system, was responsible for the Mount Painter and Mount Gee hydraulic-fracture breccias, and hydrothermal quartz deposits. This second system displays characteristics more typical of an acid sulfate system and likely to be related to a maar structure centered on Mount Painter. This system, during a later stage of cyclic temperature changes, could have included a solfatara, or other hot spring precipitates, at the ancient surface level. These native sulfur-bearing rocks on Mount Painter represent the ground surface at the time of deposition, agreeing with earlier work (e.g., Coats and Blisset, 1971) based on the proposed (but unconfirmed) sinter deposits.

The PIMA's ability to detect mineral changes on spot surface measurements was also tested and shown to contribute accurate data to the large-scale mineralogical maps. The combined study of PROBE-1 and PIMA II infrared spectra was able to demonstrate that these instruments, capable of making detailed mineralogical maps on Earth, could also be applied to finding and mapping hydrothermal alteration and mineral assemblages on Mars.

ACKNOWLEDGMENTS

We are very grateful to the Anglo-American Corporation of Johannesburg for the provision of HyMap data, and to CSIRO in Sydney for lending us a PIMA spectrometer. This project would not have been possible without the advice and computing support of CSIRO's Mineral Mapping Technologies Group in Sydney, especially Jonathon Huntington, Melissa Quigley, Peter Mason, and Kai Yang. Margaret and Douglas Sprigg of Arkaroola permitted ready access to all areas of their property, despite the inconvenience that it sometimes caused, and Doug flew us over our field area to give us the benefit of an aerial reconnaissance. Ian Plimer kindly provided a sample from a solfatara deposit on the island of Milos. This work was supported by grants from the Australian Research Council and Macquarie University.

ABBREVIATIONS

PIMA, portable infrared mineral analyzer; ROI, region of interest; SWIR, short-wave infrared; TIR, thermal infrared; VNIR, visible and near-infrared.

REFERENCES

Bock, G.R. and Goode, J.A., eds. (1996) *Evolution of Hydrothermal Ecosystems on Earth (and Mars?), Ciba Foundation Symposium 202*, John Wiley & Sons, Chichester, UK.

Cady, S.L. and Farmer, J.D. (1996) Fossilization processes in siliceous thermal springs: trends in preservation along thermal gradients. In: *Evolution of Hydrothermal Ecosystems on Earth (and Mars?), Ciba Foundation Symposium 202*, edited by G.R. Bock and J.A. Goode, John Wiley & Sons, Chichester, UK, pp. 150–173.

Clark, D.S. and Govett, G.J.S. (1990) Southwest Pacific epithermal gold: a rock-geochemistry perspective. *J. Geochem. Explor.* 35, 225–240.

Coats, R.P. and Blissett, A.H. (1971) Regional and economic geology of the Mount Painter province. *S. Aust. Geol. Survey Bull.* 43, 1–426.

Corbett, G.J. and Leach, T.M. (1994) *Southwest Pacific Rim Gold-Copper Systems: Structure, Alteration, and Mineralization*, Special Publication No. 6, Society of Economic Geologists, Littleton, CO.

Cristensen, P.R., Bandfield, J.L., Clark, R.N., Edgett, K.S., Hamilton, V.E., Hoefen, T., Kieffer, H.H., Kuzmin, R.O., Lane, M.D., Malin, M.C., Morris, R.V., Pearl, J.C., Pearson, R., Roush, T.L., Ruff, S.W., and Smith, M.D. (2000) Detection of crystalline hematite mineralisation on Mars by the Thermal Emission Spectrometer: evidence for near-surface water. *J. Geophys. Res.* 105, 9623–9642.

Dando, P.R., Thomm, M., Arab, H., Brehemer, M., Hooper, L.E., Jochimsen, B., Schlesner, H., Stor, R., Miquel, J.C., and Fowler, S.W. (1998) Microbiology of shallow hydrothermal sites off Palaeochori Bay, Milos (Hellenic Volcanic Arc). *Cah. Biol. Mar.* 39, 369–372.

Drexel, J.F. and Major, R.B. (1990) Mount Painter uranium-rare earth deposits. In: *Geology of the mineral deposits of Australia and Papua New Guinea*, Volume 2, Monograph Series-Australasian Institute of Mining and Metallurgy. 14, 993–998.

Eugster, H.P. and Jones, B.F. (1967) Gels composed of sodium–aluminum silicate, Lake Magadi, Kenya. *Science* 161, 160–163.

Foster, D.A., Murphy, J.M., and Gleadow, J.W. (1994) Middle Tertiary hydrothermal activity and uplift of the northern Flinders Ranges, South Australia: insights from apatite fission-track thermochronology. *Aust. J. Earth Sci.* 41, 11–17.

Fournier, R.O., Thompson, J.M., Cunningham, C.G., and Hutchinson, R.A. (1991) Conditions leading to recent small hydrothermal explosion at Yellowstone National Park. *Geol. Soc. Am. Bull.* 103, 1114–1120.

Francis, P.W., Thorpe, R.S., Brown, G.C., and Glasscock, J. (1980) Pyroclastic sulfur eruption at Poas Volcano, Costa Rica. *Nature* 283, 754–756.

Heald, P., Foley, N.K., and Hayba, D.O. (1987) Comparative anatomy of volcanic-hosted epithermal deposits: acid-sulfate and adularia-sericite types. *Econ. Geol.* 82, 1–26.

Huntington, J.F. (1996) The role of remote sensing in finding hydrothermal mineral deposits on Earth. In: *Evolution of Hydrothermal Ecosystems on Earth (and Mars?), Ciba Foundation Symposium 202*, edited by G.R. Bock and J.A. Goode, John Wiley & Sons, Chichester, UK, pp. 214–235.

Idnurum, M. and Heinrich, C.A. (1993) A palaeomagnetic study of hydrothermal activity and uranium mineralisation at Mt Painter, South Australia. *Aust. J. Earth Sci.* 40, 87–101.

Kokaly, R.F., Clark, R.N., and Livo, K.E. (1998) Mapping the biology and mineralogy of Yellowstone National Park using imaging spectroscopy. In: *Summaries of the 7th JPL Airborne Earth Science Workshop*, JPL publication 97–21, Jet Propulsion Laboratory, Pasadena, CA, pp. 245–250.

Kruse, F.A. (1994) Imaging spectrometer data analysis—a tutorial. *Proc. Int. Symp. Spectral Sensing Res.* 1, 44–50.

Kusakabe, M., Hayashi, N., and Kobayashi, T. (1986) Genetic environments of the banded sulfur sediments at the Takeyama Volcano, Japan. *J. Geophys. Res.* 91, 12159–12166.

Kusakabe, M., Komoda, Y., Takano, B., and Abiko, T. (2000) Sulfur isotopic effects in the disproportionation reaction of sulfur dioxide in hydrothermal fluids: implications for the $\delta^{34}S$ variations of dissolved bisulfate and elemental sulfur from active crater lakes. *J. Volcanol. Geotherm. Res.* 97, 287–307.

Lambert, I.B., Drexel, J.F., Donnelly, T.H., and Knutson, J. (1982) Origin of breccias in the Mount Painter area, South Australia. *J. Geol. Soc. S. Aust.* 29, 115–125.

Linton, P. (1998) The application of airborne hyperspectral imagery to geological exploration [abstract]. In: *Abstracts of the 14th Australian Geological Convention*, Geological Society of Australia, Sydney, p. 49.

Morris, R.V., Golden, D.C., and Bell, J.F., III (1997) Low-temperature reflectivity spectra of red hematite and the color of Mars. *J. Geophys. Res.* 102, 9125–9133.

Rinker, J.N. (1994) ISSSR tutorial introduction to spectral remote sensing. *Proc. Int. Symp. Spectral Sensing Res.* 1, 5–19.

Saunders, J.A. (1994) Silica and gold textures in Bonanza ores of the sleeper deposit, Humbolt County, Nevada: evidence for colloids and implications for epithermal ore-forming processes. *Econ. Geol.* 89, 628–638.

Wang, Q., Guo, X., and Wang, R. (1998) Lithological discrimination using hyperspectral remote sensing. *Proc. SPIE* 3502, 87–93.

Wellman, P. and Greenhalgh, S.A. (1988) Flinders/Mt Lofty Ranges, South Australia: their uplift, erosion, and relationship to crustal structure. *Trans. R. Soc. S. Aust.* 112, 11–19.

White, N.C. and Hedenquist, J.W. (1990) Epithermal environments and styles of mineralisation: variations and their causes, and guidelines for exploration. *J. Geochem. Explor.* 36, 445–474.

Yang, K., Huntington, J.F., Browne, P.R.L., and Ma, C. (2000) An infrared spectral reflectance study of hydrothermal alteration minerals from the Te Mihi sector of the Wairakei geothermal system, New Zealand. *Geothermics* 29, 377–392.

Address reprint requests to:
Prof. Malcolm R. Walter
Australian Centre for Astrobiology
Department of Earth and Planetary Sciences
Macquarie University
North Ryde, NSW 2109, Australia

E-mail: malcolm.walter@mq.edu.au

This article has been cited by:

1. Juncal A. Cruz, Nuria Sánchez-Pastor, Alexander M. Gigler, Lurdes Fernández-Díaz. 2011. Vaterite Stability in the Presence of Chromate. *Spectroscopy Letters* **44**:7-8, 495-499. [CrossRef]
2. Joël Brugger, Pierre-Alain Wülser, John Foden. 2011. Genesis and Preservation of a Uranium-Rich Paleozoic Epithermal System with a Surface Expression (Northern Flinders Ranges, South Australia): Radiogenic Heat Driving Regional Hydrothermal Circulation over Geological Timescales. *Astrobiology* **11**:6, 499-508. [Abstract] [Full Text HTML] [Full Text PDF] [Full Text PDF with Links]
3. Jonathan D. A. Clarke, Carol R. Stoker. 2011. Concretions in exhumed and inverted channels near Hanksville Utah: implications for Mars. *International Journal of Astrobiology* **10**:03, 161-175. [CrossRef]
4. Dorothy Z. Oehler, François Robert, Malcolm R. Walter, Kenichiro Sugitani, Anders Meibom, Smail Mostefaoui, Everett K. Gibson. 2010. Diversity in the Archean Biosphere: New Insights from NanoSIMS. *Astrobiology* **10**:4, 413-424. [Abstract] [Full Text HTML] [Full Text PDF] [Full Text PDF with Links]
5. Michael D. West, Jonathan D.A. Clarke, Jennifer H. Laing, David Willson, James M.A. Waldie, Guy M. Murphy, Matilda Thomas, Graham A. Mann. 2010. Testing technologies and strategies for exploration in Australian Mars analogues: A review. *Planetary and Space Science* **58**:4, 658-670. [CrossRef]
6. Michael D. West, Jonathan D.A. Clarke, Matilda Thomas, Colin F. Pain, Malcolm R. Walter. 2010. The geology of Australian Mars analogue sites. *Planetary and Space Science* **58**:4, 447-458. [CrossRef]
7. Brown AJ, Walter MR, Cudahy TJ. 2005. Hyperspectral imaging spectroscopy of a Mars analogue environment at the North Pole Dome, Pilbara Craton, Western Australia. *Australian Journal of Earth Sciences* **52**:3, 353-364. [CrossRef]
8. Adrian Brown, Malcolm Walter, Thomas Cudahy. 2004. Short-Wave Infrared Reflectance Investigation of Sites of Paleobiological Interest: Applications for Mars Exploration. *Astrobiology* **4**:3, 359-376. [Abstract] [Full Text PDF] [Full Text PDF with Links]
9. 2003. Astrobiology Literature Watch. *Astrobiology* **3**:2, 429-435. [Citation] [Full Text PDF] [Full Text PDF with Links]